Synthesis and Characterization of Mo−SBA-1 Cubic Mesoporous Molecular Sieves

Shunai Che,[†] Yasuhiro Sakamoto,[‡] Hideaki Yoshitake,[§] Osamu Terasaki,[‡] and Takashi Tatsumi*[,†]

Division of Materials Science & Chemical Engineering, Faculty of Engineering, Yokohama National University, 79-5 Tokiwadai, Hodogayaku, Yokohama 240-8501, Japan, Department of Physics, Graduate School of Science and Center of Interdisciplinary Research, Tohoku University, Sendai, 980-77, Japan, and CREST Science and Technology Corporation, Japan, and Institute of Environmental Science, Yokohama National University, 79-5 Tokiwadai, Hodogayaku, Yokohama 240-8501, Japan

Received: June 13, 2001; In Final Form: August 25, 2001

A series of Mo−SBA-1 ($Pm\bar{3}n$) cubic mesoporous molecular sieves with various H_2O/HCl and Si/Mo molar ratios have been synthesized at 0 °C using cetyltriethylammonium bromide, tetraethyl orthosilicate, ammonium heptamolybdate and hydrochloric acid. It was found that the Mo−SBA-1 particles synthesized at 0 °C for 4 days were of a characteristic shape having fifty-four, seventy-four, or more crystal faces. Synthesis conditions have been optimized to introduce high percentage of Mo into the well-ordered cubic mosoporous structure. The microstructure of Mo centers has been investigated by diffuse reflectance UV−visible and laser Raman spectroscopies. Both techniques reveal that, in the absence of water, Mo species consist of tetrahedrally and octahedrally coordinated monomers and polymers. The tetrahedral Mo centers were converted to octahedral Mo centers in the presence of moisture partially in directly synthesized Mo−SBA-1 samples and completely in impregnated Mo/SBA-1 samples. It is concluded that the impregnated samples were better dispersed than the directly synthesized samples.

Introduction

Since the discovery of the M41S family of mesoporous molecular sieves with surface areas often over 1000 m^2/g and well-ordered pore sizes that are substantially larger than in zeolites, a great deal of interest has been focused on their applications as high pore volume catalysts, adsorbents or host structures for nanometer-sized guest compounds.[1−6] The initial forms of the M41S family and analogous mesoporous materials were synthesized as silicates. Because of its special pore structure, subsequent synthesis efforts have been made to produce mesoporous materials having heteroatom substitutions, e.g., Ti,[7,8] V,[9−11] Mn,[12,13] Al,[14−19] Fe,[20,21] Cu,[22,23] Zr,[24] Cr, [25] W,[26,27a] Pt,[27b]and Mo[27a,27c,] onto or within the silica wall. Molybdenum dispersed on high surface area oxide supports has many applications in industrial catalysis, and the synthesis and characterization of such catalysts has been attracting wide attention. For example, selective oxidation of hydrocarbons,[28] olefin metathesis,[29] and mixed alcohol formation from CO and H_2O have been widely studied using molybdenum oxide catalysts.

A cubic phase SBA-1 ($Pm\bar{3}n$) possesses three dimensional (3D) channel systems with uniformly sized pore structure of cage type with open windows.[31] Because of the high surface area, high thermal stability and, especially, three-dimensional channel connectivity, SBA-1 is considered to be suitable for a catalyst support.[32−38] Up to now, surprisingly little research has been reported on SBA-1, compared with other mesoporous materials such as 2D hexagonal (*p6 mm)* MCM-41 or SBA-3.

Huo et al.[27c,32,33] reported that the silica mesophases of the SBA-1 can be formed using a combination of cationic surfactant (S^+), halogen anion (X^-), and cationic silicate species (I^+), through the acidic route. Large headgroup surfactants such as alkyltriethylammonium $C_nH_{2n+1}(C_2H_5)_3N^+$ (n = 12, 14, 16, and 18) favored the SBA-1 cubic $Pm\bar{3}n$ mesophase. Highly ordered mesophases can be formed over a wide range of strongly acidic conditions. They found that HCl favors the formation of SBA-1 cubic mesophase. Kim and Ryoo[37] have found that low temperature was favorable for the formation of the high quality cubic mesophase. Recently, Kruk et al.[38] reported that nitrogen adsorption showed that highly ordered SBA-1 materials exhibited broad steps of capillary condensation on N_2 adsorption−desorption isotherms and broad pore size distributions, which may be related to a cagelike pore structure of these materials.

Morey et al.[27c] have synthesized Mo−SBA-1; however, when $MoCl_5$ (aq) was added at a Si /Mo molar ratio of 16, only 0.4 at. % Mo was incorporated. Despite the potential for an excellent support, metal loading has not reached a level of interest because the acidity employed for the synthesis leads to the high solubility of metal precursors, which retards their incorporation into SBA-1.

We have already reported that high quality SBA-1 materials show a highly isotropic morphology having fifty-four or more crystal faces.[39] Here, we report high incorporation of Mo into the SBA-1 mesophases under varying synthetic conditions. Mo incorporated mesoporous SBA-1 with Si/Mo molar ratio as low as 23 with highly ordered cubic structure retained was synthesized by adjusting the H_2O/HCl and Si/Mo molar ratios of starting gels. Using UV−vis and Raman spectroscopies the structure of molybdenum species and their interaction with

* To whom correspondence should be addressed. Telephone: (81)45-339-3941. Fax: (81)45-339-3941. E-mail: ttatsumi@ynu.ac.jp.

[†] Division of Materials Science & Chemical Engineering, Faculty of Engineering, Yokohama National University.

[‡] Department of Physics, Graduate School of Science and CREST, JST, Tohoku University.

[§] Institute of Environmental Science, Yokohama National University.

10.1021/jp012230l CCC: $20.00
Published on Web 10/09/2001

framework silica was investigated; comparison was made between the direct incorporation during the synthesis (Mo−SBA-1) and postsynthesis impregnation of mesoporous silica (Mo/SBA-1).

Experimental Section

Surfactant Preparation. Cetyltriethylammonium bromide (CTEABr) was synthesized by the reaction of cetyl bromide ($C_{16}H_{33}Br$) with triethylamine ($(C_2H_5)_3N$) both from TCI, Japan; $C_{16}H_{33}Br$ (0.5 mol) was added to $(C_2H_5)_3N$ (0.75 mol) in acetone (400 mL). The reaction mixture was stirred for 7 days under reflux conditions. The product was decanted and purified by recrystallization from an acetone solution. The resulting product was separated by filtration and dried under vacuum for several hours at 60 °C.

Synthesis of Mo−SBA-1. Mo−SBA-1 cubic mesoporous silica was synthesized under various conditions using CTEABr as the surfactant, tetraethyl orthosilicate (TEOS, from TCI, Japan) as a silica source and ammonium heptamolybdate (AHM) as a molybdenum source in hydrochloric acid. The molar composition of the reaction mixture was 0.13 CTEABr:1 TEOS:*x* HCl:125 H_2O:*y* AHM, where *x* and *y* were varied in the range of 10−1.25 and 0−0.028, respectively. The pH values were lower than 2. Synthesis was performed as follows. Aqueous solution of AHM was prepared first. CTEABr, distilled water, and hydrochloric acid were mixed to obtain a homogeneous solution, which was cooled to 0 °C prior to the addition of TEOS and molybdenum precursor. TEOS and AHM solution were also precooled to 0 °C. When the mixture became clear, TEOS and AHM were added consecutively while the mixture was being vigorously stirred. The mixture was stirred for 3 min and then allowed to react at 0 °C under static conditions for 4 days. The resultant pale yellow precipitates were filtered (without washing), and dried at 100 °C overnight. Surfactants were removed by calcination in air under static conditions at 630 °C for 4 h to give Mo−SBA-1 samples. For comparison, Mo/SBA-1 was prepared by impregnating the pure silica SBA-1 with an aqueous solution (pH ∼5) of AHM at room temperature for 2 h followed by evaporation to dryness. The sample was dried at 100 °C for 12 h and calcined at 630 °C for 4 h. The loading amount of molybdenum was Si/Mo = 80.

Characterization. XRD patterns were recorded using an MX Labo powder diffractometer equipped with Cu Kα radiation (40 kV, 20 mA) at the rate of 1.0 deg/min over the range of 1.5−10.0 °(2θ). The samples were prepared as thin layers on glass slides.

Inorganic elemental analyses were performed on a Shimadzu ICP-8000E emission photometer.

SEM images were taken using a JXA-8900RL electron probe X-ray microanalyzer. For the SEM observations, the samples were deposited on a sample holder and coated with Pt.

HRTEM images were taken on a JEM-3010 microscope operating at an accelerating voltage of 300 kV. For TEM measurements, all Mo−SBA-1 materials were crushed in an agate mortar, dispersed in ethanol, and deposited on a microgrid.

N_2 adsorption−desorption isotherms were measured at −196 °C on a Belsorp 28SA sorptionmeter. Samples were pretreated for 2 h at 200 °C and 1.33×10^{-4} Pa. The BET specific surface area S_{BET} was calculated using adsorption branches in the relative pressure range from 0.04 to 0.1. The primary mesopore volume V_p was obtained using the high-resolution *t*-plot method. The pore size distribution were calculated from adsorption branches of isotherms using the BJH method, with the corrected Kelvin equation proposed recently.[38,40−43]

TABLE 1: Synthesis Results of Various Mo Introduced Mesoporous Silica

mesoporous silica	MCM-48[a]	MCM-41[b]	HMS[c]		SBA-3[d]		
pH of synthesis gel	∼11	∼11	∼7	∼7	∼2	∼2	∼2
Si/Mo (mol) of starting gel	20	20	20	50	20	50	100
Si/Mo (mol) of product	1600	2300	55	131	16	49	70

[a] MCM-48 (cubic, $Ia\bar{3}d$) synthesized at 100 °C for 10 days using 1 TEOS:0.7 CTMACl:0.3 CTMAOH:46.5 H_2O:0.0071 AHM. See ref 8a. [b] MCM-41 (hexagonal, *p6mm*) synthesized at 100 °C for 10 days using 1 TEOS:0.7 CTMACl:0.3 CTMAOH:46.5 H_2O:0.0071 AHM. See ref 8b. [c] HMS (hexagonal, *p6 mm*) synthesized at room temperature for 4 days using 1 TEOS:0.2 $C_{12}H_{25}NH_2$:150 H_2O:6 C_2H_5OH:0.0071 or 0.0028 AHM. See ref 43. [d] SBA-3 (hexagonal, *p6mm*) synthesized at room temperature for 4 days using 1 TEOS:0.2 CTMABr:150 H_2O:1 HCl:0.0071, 0.0028, or 0.0014 AHM. See refs 33, 35, and 44.

UV−vis diffuse reflectance spectra were recorded with a Varian DMS 300 UV−vis spectrometer. Samples were scanned after dehydration and hydration treatments. The dehydration was conducted by evacuation at 200 °C for 2 h. Completely wet powder treated with distilled water were used as hydrated samples. Samples were placed in quartz sell and dehydrated $MgSO_4$ calcined at 300 °C for 3 h was used as a reference.

Laser Raman spectra were taken on a JASCO NRS-2000 Raman microscope with the 514.5 nm emission of an Ar^+ laser at room temperature. The samples were pressed into wafers and irradiated in air. The incident laser power at the samples was 30 mW. The scattered photons were passed through a double monochlometer to an optical multichannel analyzer. Slit width was typically 200 μm.

Results and Discussion

Synthesis of Mo-Containing Mesoporous Silica under Various pH Conditions. Mesoporous silica can be synthesized under alkaline,[1−6] acidic,[31−38] and neutral[43] conditions. First, Mo was introduced into various mesoporous silica during their synthesis process using AHM as a Mo source. As shown in Table 1, Mo was difficult to be incorporated into mesoporous silica under basic conditions. In contrast, acidic synthesis is favorable for the incorporation of Mo. Most Mo in the mother gel was incorporated into the SBA-3 mesophase. The synthesis under neutral conditions (HMS) showed the intermediate behavior; about 40% of Mo was incorporated into the HMS structure. From XRD pattern, N_2 adsorption−desorption, and SEM images (not shown), it was confirmed that the mesostructures of MCM-48, MCM-41 and HMS were not influenced by the presence of Mo, while that of the SBA-3 became disordered with increasing Mo amount (Si/Mo ≤ 50).

In aqueous solutions, Mo exists as anions under all of the pH conditions. Under basic conditions, the silicate species is negatively charged, causing repulsion of the oxoanions of Mo and, therefore, limiting the introduction of Mo species into the silica framework. Thus, the basic conditions are not suitable for the synthesis of mesostructures incorporating Mo.

Synthesis of Mo−SBA-1 from the Gel with Various H_2O/HCl Molar Ratios. So far, the 3D cubic phase MCM-48 ($Ia\bar{3}d$) had not been synthesized under acidic conditions. Since the SBA-1 phase possessing 3D channel systems is synthesized under acidic conditions, we attempted to incorporate Mo into the SBA-1 phases. The properties of the Mo−SBA-1 samples synthesized with various H_2O/HCl molar ratios (12.5−100) at 0 °C for 4 days are collected in Table 2. The starting Si/Mo

TABLE 2: Properties of Calcined Mo−SBA-1 Samples Synthesized with Various H_2O/HCl Molar Ratios

synthesis conditions H_2O/HCl (mol)	product Si/Mo molar ratio[a]	unit cell *a*/nm	Si base yield %	surface area S_{BET}/m^2 g^{-1}	primary mesopore vol V_p/mm^3 g^{-1}	pore diameter d_{BJH}/nm
12.5	490	7.5	86.1	964	466	2.9
25	380	7.6	78.1	991	476	2.8
50	320	7.7	74.5	1025	498	2.8
75	120	7.7	67.1	1088	513	2.8
100	80	6.8	50.3	1118	498	2.6

[a] The starting Si/Mo molar ratio is 50.

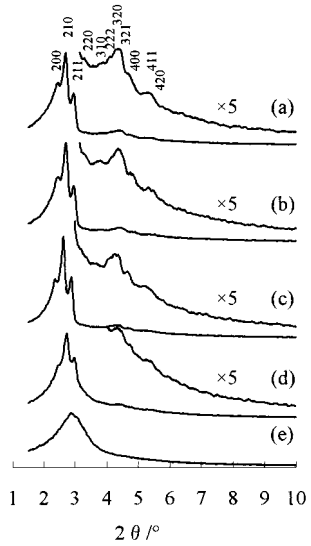

Figure 1. XRD patterns of calcined Mo−SBA-1 with various H_2O/HCl molar ratios at 0 °C for 4 days. Synthesis molar composition: 0.13 CTEABr:1 TEOS:*x* HCl:125 H_2O:0.0028 AHM. H_2O/HCl = (a) 12.5, (b) 25, (c) 50, (d) 75, and (e) 100.

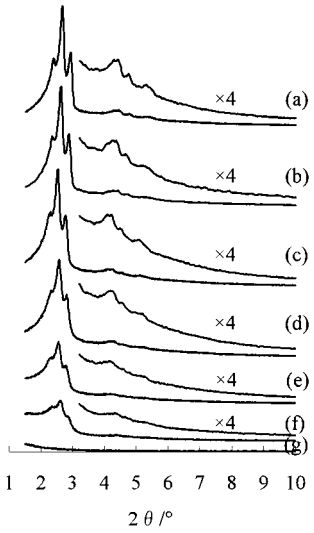

Figure 2. XRD patterns of calcined Mo−SBA-1 synthesized with different Si/Mo molar ratios at 0 °C for 4 days. Synthesis molar composition: 0.13 CTEABr:1 TEOS:2.5 HCl:125 H_2O:*x* AHM. Si/Mo = (a) 8, (b) 50, (c) 30, (d) 20, (e) 15, (f) 10, and (g) 5.

TABLE 3: Properties of Calcined Mo−SBA-1 Samples Synthesized with Various Si/Mo Molar Ratios

synthesis conditions Si/Mo (mol)	product Si/Mo molar ratio	unit cell *a*/nm	S_{BET}/ m^2 g^{-1}	primary mesopore vol V_p/mm^3 g^{-1}	pore diameter d_{BJH}/nm
∞	∞	7.5	1024	510	2.7
50.0	320.0	7.7	1025	498	2.8
30.0	221.0	7.8	1028	565	2.9
20.0	138.0	7.7	1127	604	2.8
15.0	68.0	7.7	1018	565	2.8
10.0	23.0	7.6	963	507	2.8
5.0	7.0		80	18	

molar ratio was 50. The Si/Mo molar ratio of the products was increased with decreasing H_2O/HCl molar ratio, i.e., the introduction of Mo in to SBA-1 became difficult with increasing acidity. The silica base yields were increased and the surface areas were decreased with decreasing H_2O/HCl molar ratios. The unit cell parameter and pore size were virtually unchanged.

Figure 1 shows XRD patterns of calcined Mo−SBA-1 samples. In a manner similar to the pure silica SBA-1,[39] the calcined powder synthesized with H_2O/HCl = 12.5, 25, and 50 showed XRD patterns with three well-resolved lines in the range of 2 θ = 1.5−3°, which are indexed to the 200, 210, and 211 diffractions of the SBA-1 structure, based on the cubic system.[31−37] Some additional weak peaks in the range of 3.5 to 6° corresponding to the 220, 310, 222, 320, 321, 400, 411, and 420 scattering reflections appeared, indicating that calcined Mo−SBA-1 has a high degree of cubic mesoscopic order. The XRD intensity of the samples increased with further increasing H_2O/HCl molar ratio, and Mo−SBA-1 synthesized with H_2O/HCl = 50 molar ratio showed the strongest peak intensity and the narrowest peak width, which suggest the high crystallinity of the material. The XRD intensities were decreased and the lines were merged to a single broad peak with further increase in the H_2O/HCl molar ratio through 75−100.

It is considered that the acidity of the synthesis gel is the most important parameter for the formation of SBA-1 structure and also the incorporation of molybdenum into the SBA-1. The H_2O/HCl molar ratio of 50 gave the most favorable acidity for the formation of the cubic mesostructure in the presence of molybdenum. It could be related to the fact that the concentration of [H^+] strongly influences the condensation reaction of silicate species. Cationic silicate species have ready access to soluble surfactant cation molecular species through counteranion and can readily restructure micelle arrays. Silica condensation causes the positive charge density of the silicate network to decrease. The SBA-1 mesostructure corresponds to the largest surface curvature micelle of all lyotropic liquid crystals, and the micellar surface has the lowest charge density. The organic surfactants pack to form a high surface curvature to adjust the effective headgroup area, maintaining charge matching in the interface so that the SBA-1 mesophases is formed. Once the mesophase is formed and significant condensation takes place, the mesostrucuture does not seem to be affected by the further condensation. However, as can be seen from the Si base yield (Table 1), when excess condensation of silica proceed under high [H^+] concentration, amorphous silica produced afterward existed in the SBA-1 samples, which led XRD peaks to broaden and surface areas to decrease. On the other hand, the SBA-1 mesophase could not be constructed for high charge density of silica framework caused by insufficient silica condensation under lower acidity conditions.

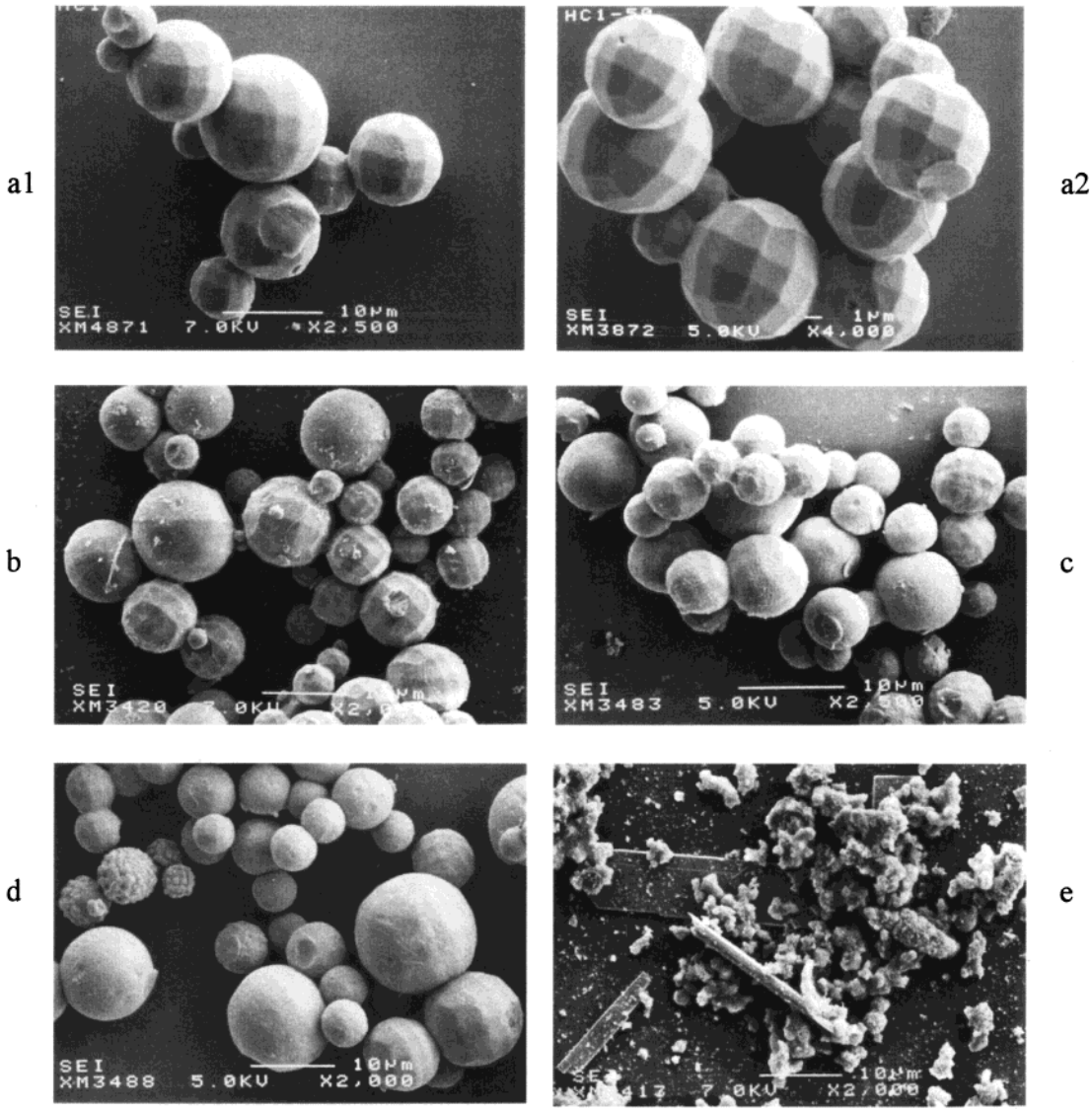

Figure 3. SEM images of calcined Mo−SBA-1 shown in Figure 1.Si/Mo = (a1 and a2) 50, (b) 20, (c) 15, (d) 10, and (e) 5.

Syntheis of Mo−SBA-1 with Various Si/Mo Molar Ratios. On the basis of the above results, the increased incorporation of Mo in the well-ordered SBA-1 structure was attempted by varying the Si/Mo ratio with the starting H_2O/HCl molar ratio set at 50. The properties of the samples are listed in Table 3. The incorporation of Mo in the product was dependent not only on the H_2O/HCl molar ratio but also on the Si/Mo molar ratio in the starting gel. The product Si/Mo ratio of 23 was achieved with the SBA-1 mesostructure kept, as shown below.

Figure 2 shows XRD patterns of calcined Mo−SBA-1 mesoporous molecular sieves prepared with various Si/Mo molar ratios (∞−5). The XRD patterns of the samples synthesized without molybdenum and with Si/Mo = 50−10 have three well-resolved peaks in the range of 2θ = 1.5−3.0 °. The unit cell parameters are almost the same (7.5−7.8 nm) as shown in Table 3. The intensities of XRD peaks of the sample were decreased with decreasing Si/Mo molar ratio of synthesis gel, which is partly due to increasing destructive interference with the mesoscopic order with increasing amounts of molybdenum oxide species. No SBA-1 cubic structure was obtained with Si/Mo = 5; MoO_3 crystals were detected from the XRD pattern. Other samples exhibited no peaks at higher angles due to molybdenum oxide clusters, indicating that Mo oxide particles synthesized within the pores and on the surfaces would be too small to give X-ray differections.

Figure 3 shows SEM images of the samples shown in Figure 2. Obviously, the regular and distinct fifty-four and seventy-four crystal faces appeared in the samples synthesized with Si/Mo = 50−10, which showed highest crystallinity as revealed by the XRD pattern. Figure 3(a2) is the magnification of particles with uniform fifty-four crystal faces. The crystal with fifty-four and seventy-four faces had four 3-fold axes and exhibited cubic symmetry. Fifty-four-face crystal faces are composed of six {100}, 24 {210}, and 24 {211} planes, and that seventy-four faces are described as the fifty-four-face crystal to which 12 elongated hexagons and eight triangles are added. The elongated hexagons and triangle are {110} and {111} planes in the cubic structure, respectively. The rodlike materials in samples of Si/Mo = 5 seem to be MoO_3 crystals.

Five samples synthesized with Si/Mo molar ratio = 50, 30, 20, 15, and 10 were studied by HRTEM. Three electron diffraction patterns of the same crystallite (the [100], [110], [111], and [210] directions) are presented in Figure 4 for the sample synthesized with Si/Mo = 10. The corresponding Fourier diffractogram shown in the inset indicates extinction conditions for the reflections. The images revealed regular periodicity over very large areas and this clearly indicates the crystal is a single

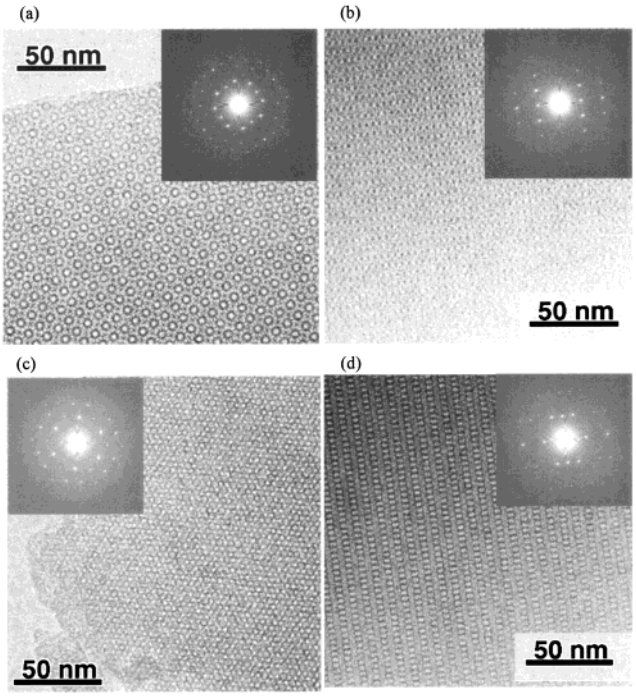

Figure 4. HREM images and their Fourier diffractograms of calcined Mo−SBA-1 sample. (a) [100], (b) [110], (c) [111], and (d) [210].

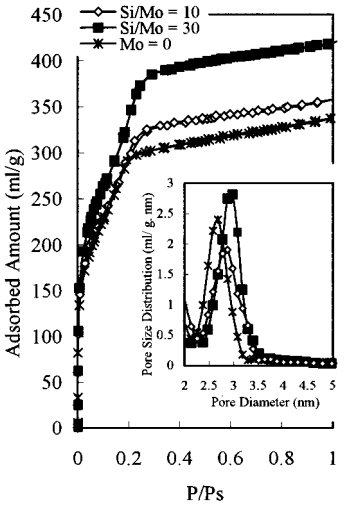

Figure 5. N_2 adsorption−desorption isotherms and pore size distributions of calcined Mo−SBA-1 synthesized with different Si/Mo molar ratios at 0 °C for 4 days. Synthesis molar composition is the same as that for Figure 2.

crystal with well-ordered mesostructure. The $Pm\bar{3}n$ space group with the same mesostructure as previous reported[31] was confirmed by an analysis of a set of HRTEM images. The EM experiments indicated that the particles are remarkably perfect single crystals. It has been confirmed that the samples with well-resolved XRD patterns exhibit similar HREM images regardless of its content of molybdenum.

All the samples with well-ordered SBA-1 cubic structure give similar IV type adsorption−desorption isotherms of N_2[45] (Figure 5). All of the samples exhibit a clearly defined peak at 2.7−2.9 nm (full width at half-maximum ∼0.4 nm) in the pore size distribution (Figure 5, in set). It is considered that a high quality SBA-1 cubic structure can be still retained at high Mo contents. However, the N_2 adsorption−desorption isotherms exhibited a broad capillary condensation step for each sample compared to MCM-41 or MCM-48, despite high periodicity of the structure

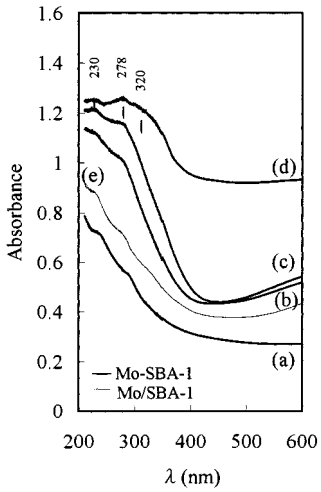

Figure 6. UV−vis diffuse reflectance spectra for Mo−SBA-1 and Mo/SBA-1. Mo−SBA-1: Mo introduced directly with various Si/Mo molar ratios. The product Si/Mo molar ratios are (a) 221, (b) 138, (c) 68, and (d) 23. Mo/SBA-1: Mo introduced by impregnation with (e) Si/Mo = 80 molar ratio.

of SBA-1, as implied from the XRD data. This result may be due to its cagelike pores of two types, namely, the variation of pore size in the pore channel. However, since the BJH calculations are based on the assumption of cylindrical pore geometry, the BJH data are not sufficient to draw a definite conclusion about the presence of cagelike type of SBA-1. We observed only one peak in our pore size analysis despite that there are two types of pore in SBA-1 mesophase; probably two peaks have coalesced because the ratio of two pore size diameter was only ∼1.1.[46]

The surface area (∼1000m^2/g) and pore diameters (2.7−2.9 nm) were virtually unchanged (Table 3), indicating that there was no great difference in pore structure among the samples synthesized with various Si/Mo molar ratios, despite the different Mo content.

For comparison, Mo was also introduced by impregnation of pure silica SBA-1 with a solution of AHM to obtain Mo/SBA-1 with various Si/Mo molar ratios. From XRD patterns, SEM images, and N_2 adsorption−desorption (not shown), it was observed that the SBA-1 mesostructure was maintained in the range of Si/Mo molar ratio ≥10. In the lower range of Si/Mo ratio of 30−10, the XRD intensities were decreased with increasing amount of Mo, and amorphous materials were obtained with further increasing amount of Mo.

Diffuse Reflectance UV−Vis and Raman Characterization. Diffuse reflectance UV−vis spectroscopy is quite a potential method for determining local molecular coordination sphere and bonding information for inorganic compounds. UV−vis diffuses reflectance spectra of dehydrated Mo−SBA-1 mesoporous molecular sieves prepared from the starting solution of various Si/Mo molar ratios are shown in Figure 6. Oxomolybdenum compounds give absorption bands in UV−vis region due to ligand−metal charge transfer (O^{2-}−Mo^{6+}). The position of this electronic transition depends on the ligand field symmetry surrounding the Mo center; the tetrahedral Mo^{6+}(T_d) is expected to show a higher energy transition than for the octahedral one.[47] Absorption bands around 230 nm may be due to the contributions of octahedral and tetrahedral Mo^{6+}. Bands from 250 to 280 nm have been assigned to Mo^{6+} ($T_d(t_1 \rightarrow e)$) and bands from 300 to 330 nm to Mo^{6+} ($O_h(t_{2u},t_{1g} \rightarrow t_{2g})$).[48−52] The ratios of absorbance at 230 nm to that at 278 nm decreased with increasing Si/Mo. Mo−SBA-1 with Si/Mo = 23 gave three

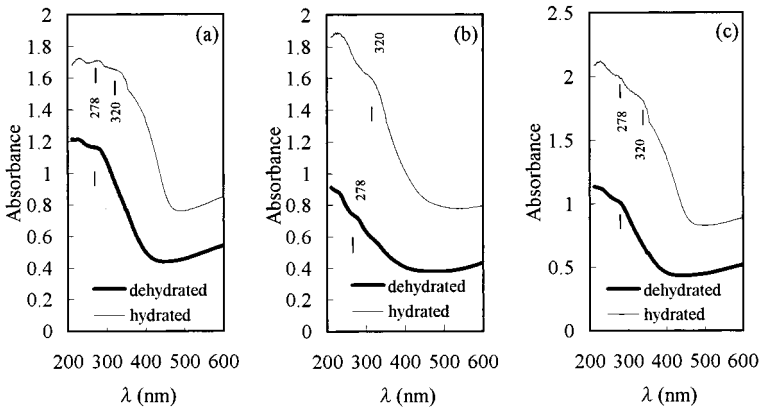

Figure 7. Ultraviolet-visible diffuse reflectance spectra for Mo−SBA-1 and Mo/SBA-1. (a Mo−SBA-1, Si/Mo = 68; (b) Mo/SBA-1, Si/Mo = 80; and (c) Mo−SBA-1, Si/Mo = 138.

bands at 230, 278, and 320 nm. The last one was invisible when Si/Mo was beyond 68 for both directly synthesized and impregnated samples. The band at 320 nm for the sample with Si/Mo = 23 indicated the presence of octahedral molybdenum species.

The disappearance of the marker at 320 nm in the low Si/Mo region suggested that lack of octahedral molybdenum in low Mo loadings. It is likely that most of Mo were fixed in the silica lattice of SBA-1. Weber showed the linear relationship between the position of UV-absorption edge and the number of next nearest neighbors of the Mo compounds.[47] The edge energies, calculated according to his proposition, were 3.0, 3.6, 3.8, and 3.8 for Si/Mo = 23, 68, 138, and 221, respectively. Thus, the numbers of next nearest neighbors were estimated at 4.5, 1.6, 1.2, and 1.2, respectively. The lowest energy of 3.0 eV agrees well with that of bulk MoO_3,[47] which suggests the most of molybdenum species present grew up to the bulky oxide in the high Mo loading sample with Si/Mo = 23. The higher UV absorption edges 3.6 and 3.8 eV corresponded to the energies between $[Mo_7O_{24}]^{6-}$ (=3.3 eV) and $[Mo_2O_7]^{2-}$ (=3.9 eV),[47] which strongly suggests aggregation of molybdate ions occurring during the preparation of Si/Mo = 68, 138, and 221 samples. As the loading increased, the ions aggregated to a great extent.

After dehydration by heating under vacuum the color of all the samples changed from pale yellow-green to gray, indicating that Mo^{5+} ion was generated.[53] There was no band in the visible region of 400−500 nm. This is not surprising because the d−d transitions of Mo^{5+}(O_h($^2T_{2g}\rightarrow {}^2E_g$), C_{4v}($b_{2g}\rightarrow b_{1g}$)) and Mo^{5+} (T_d ($^2E\rightarrow {}^2T$)) are weaker than those of the charge-transfer transition.

The rehydration behavior of Mo−SBA-1 and Mo/SBA-1 are compared in Figure 7. After rehydration, the color changed again from gray to green. For Mo/SBA-1, the adsorption at 278 nm assigned to tetrahedral Mo^{6+} (T_d($t_1\rightarrow$ e)) was masked behind that at 320 nm, a characteristic band of octahedral Mo^{6+} (O_h(t_{2u},$t_{1g}\rightarrow t_{2g}$)), which is possibly due to the coordination of water molecule. As discussed below, the strong Raman bands appearing around 900 cm^{-1} suggest that Mo^{6+} (T_d) is highly dispersed on Mo/SBA-1 catalyst easily bound to water in the presence of moisture. In contrast, the 278 nm band was still observed on rehydrated Mo−SBA-1 samples, despite the growth of that of 320 nm. This indicates that a large part of Mo, which is probably strongly fixed in the framework of SBA-1, is hardly coordinated by water and the rehydration is limited to the atoms that are reactive on the surface.

From the X-ray diffraction patterns, noticeable structural differences were observed neither between Mo−SBA-1 and Mo/SBA-1 nor between hydrated and dehydrated states. The nature of the interaction between the MoO_4^{2-} centers incorporated via (Mo−O−Si) bridges existing in the framework and the surfaces and the silica walls are, therefore, not strongly affected by exposure to moisture.

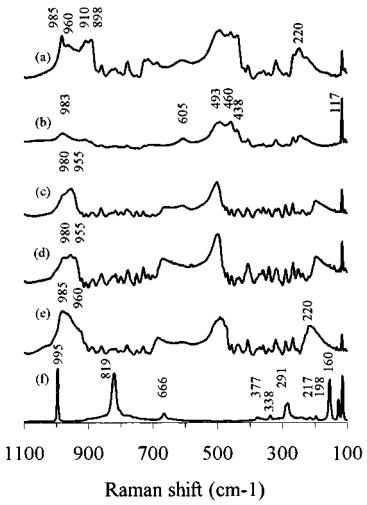

Figure 8. Raman spectra for calcined samples of (a) Mo/SBA-1 (Si/Mo = 80), (b) SBA-1 (pure silica), and (c−f) Mo−SBA-1 (Si/Mo = 138, 68, 23 and 7).

Figure 8 presents the Raman spectra of calcined pure SBA-1; Mo−SBA-l with Si/Mo = 7, 23, 68, and 138; and of calcined Mo/SBA-1 with Si/Mo = 80. The spectrum of the sample with Si/Mo = 7 was dominated by the sharp peaks characteristic of MoO_3 appearing at 995, 819, 666, 377, 338, 291, 248, 217, 198, and 160 cm^{-1},[54] whereas these bands could not be detected in the other spectra. However, in the microscope Raman mode, it was found that the surface was uniform and there were no particular particle of MoO_3 producing the scattering pattern of (e), despite that bulk MoO_3 was observed from UV−vis spectra of Mo−SBA-1 (Si/Mo = 23). This microscopic feature demonstrates the presence of highly dispersed MoO_3 in Mo−SBA-1. Other evidence for the good dispersion comes from the X-ray diffraction pattern, in which the peak corresponding to crystalline MoO_3 was observed for neither Mo−SBA-1 nor Mo/SBA-1, indicating that the MoO_3 aggregates must be extremely small. Broad bands at 980, 605, and 500−300 cm^{-1} in addition to a sharp peak at 117 cm^{-1} are the characteristics of SiO_2, which were observed in the purely siliceous SBA-1 (Figure 8b).

Fully oxidized molybdenum can be tetrahedrally or octahedrally coordinated. We discussed the oxygen coordination of Mo^{6+} species in UV−vis spectra. However, it is difficult to

differentiate octahedral Mo^{6+} (O_h) and tetrahedral Mo^{6+} (T_d) from Raman spectra because both octahedral (O_h) and tetrahedral (T_d) species have Raman bands for the Mo−O stretch in the 800−1000 cm^{-1} region. Therefore, it is not possible to discriminate structures solely on the basis of Mo−O stretching band position; however, the frequency of the Mo−O stretching mode is dependent on the length of the Mo−O bond.[55]

Mo−O stretching vibration was associated with bands above 900 cm^{-1}, and the bands appearing at 860 cm^{-1} (for $Mo_8O_{26}^{4-}$) and 564 cm^{-1} (for $Mo_7O_{24}^{6-}$) are typical asymmetric stretchings of Mo−O−Mo bond.[52] The latter bands were not found in Mo−SBA-1 expect that with Si/Mo = 7 (MoO_3). The intensity of this scattering is usually weak. It is likely that the noise or the scattering from silica covered up this region in the spectra (a), (c), (d), and (e). In the region between 900 and 1000 cm^{-1}, the spectra appeared as a combination of the bands from silica (ca. 980 cm^{-1}) and Mo−O asymmetric stretching of molybdate. The position of the latter component is strongly dependent on the size of Mo cluster; that is, $Mo_8O_{26}^{4-}$, $Mo_7O_{24}^{6-}$, and MoO_4^{2-} show 965, 943, and 897 cm^{-1}, respectively.[56] Namely, ν_{as}(Mo−O) is lowered with decreasing size of Mo cluster. The shoulder observed around 945 cm^{-1} in the spectrum of the Mo−SBA-1 sample with Si/Mo = 138 can be assigned to ν(Mo−O) of $Mo_7O_{24}^{6-}$ like structure, suggesting it has smaller Mo clusters than those of the Mo−SBA-1 samples with Si/Mo = 23 and 68.

For the impregnated Mo/SBA-1, two bands at 910 and 898 cm-1 appeared which is assigned to less aggregated molybdates than in Mo−SBA-1. These two bands, in agreement with the effect of hydration observed with UV−vis spectroscopy shown in Figure 7, demonstrate that molybdenum is more highly dispersed in Mo/SBA-1 than that in Mo−SBA-1.

Above observation can be explained by the state of molybdenum oxoanion in the synthesis and impregnation solutions. As mentioned in the Experimental Section, the Mo−SBA-1 was synthesized under highly acidic conditions (pH < 2), and the Mo/SBA-1 were prepared by impregnation with an aqueous solution of AHM at pH ≈ 5. In aqueous solutions of molybdenum anions, different equilibrium phases exist, depending on the pH:[57−59]

$$[Mo_7O_{24}]^{6-} + 3H^+ + [HMoO_4]^- \rightleftarrows [Mo_8O_{26}]^{4-} + 2H_2O \quad (pH < 2) \quad (1)$$

$$7[MoO_4]^{2-} + 8H^+ \rightleftarrows [Mo_7O_{24}]^{6-} + 4H_2O \quad (2 < pH < 7) \quad (2)$$

At pH < 2, i.e., the Mo−SBA-1 synthesis conditions, the oxomolybdenum anions are present as large polyanions; the pH was low enough to convert the most of molybdate into $[Mo_8O_{24}]^{4-}$ through eq 1, resulting in poor dispersion on the silica surfaces. In the pH range of 2 to 7 i.e., the Mo/SBA-1 impregnation conditions, the molybdenum oxoanions is smaller than under low pH conditions, which leads to a better dispersion of Mo oxide on silica surfaces.

Acknowledgment. The authors are grateful to Y. Shimada (Instrumental Analysis Center, Yokohama National University) for measuring scanning electron micrographs (SEM).For financial support, O.T. thanks CREST, JST, and T.T. thanks JCII, respectively.

References and Notes

(1) Beck, J. S. U.S. Patent 5 507 296, 1991.
(2) Kresge, C. T.; Leonowicz, M. E.; Roth, W. J.; Vartuli, J. C. U.S. Patent 5 098 684, 1992.
(3) Beck, J. S. et al. U.S. Patent 5 108 725, 1992.
(4) Beck, J. S.; Vartuli, J. C.; Roth, W, J.; Leonowicz, M. E.; Kresge, C. T.; Schmitt, K. D.; Chu, C. T.-W.; Olson, D. H.; Sheppard, E. W.; McCullen, S. B.; Higgins, J. B.; Schlenker, J. L. *J. Chem. Soc.* **1992**, *114*, 10834.
(5) Ying, J. Y.; Mehnert, C. P.; Wong, M. S. *Angew. Chem., Int. Ed.* **1999**, *38*, 56.
(6) Barton, T. J.; Bull, L. M.; Klemperer, W. G.; Loy, D. A.; McEnaney, B.; Misono, M.; Monson, P. A.; Pez, G.; Scherer, G. W.; Vartuli, J. C.; Yaghi, O. M. *Chem. Mater.* **1999**, *11*, 2633.
(7) Morey, M. S.; Davidson, A.; Stucky, G. D. *Microporous Mater.* **1996**, *6*, 99.
(8) (a) Koyano, K. A.; Tatsmi, T. *Chem. Commun.* **1996**, 145. (b) Koyano, K. A.; Tatusmi, T. *Microporous Mater.* **1997**, *10*, 259.
(9) (a) Morey, M. S.; Davidson, A.; Eckert, H.; Stucky, G. D. *Chem. Mater.* **1996**, *8*, 186. (b) Van Der Voot, P.; Morey, M. S.; Davidson, A.; Stucky, G. D.; Mathieu, M.; Vansant, E. F. *J. Phys. Chem.* B **1998**, *102*, 585.
(10) Dai, L. X.; Tabata, K.; Suzuki, E.; Tatsumi, T. *Chem. Mater.* **2001**, *13*, 208.
(11) (a) Chatterjee, M.; Iwasaki, T.; Hayashi, H.; Onodera, Ebina, T.; Nagasa, T. *Chem. Mater.* **1999**, *11*, 1368. (b) Luan, Z.; Bae, J. Y. Kevan, L. *Chem. Mater.* **2000**, *12*, 3202.
(12) Zhao, D. Y.; Goldfarb, D. *J. Chem. Soc. Chem. Commun.* **1995**, 875.
(13) Xu, J.; Luan, Z.; Hartmann, M.; Kevan, L. *Chem. Mater.* **1999**, *11*, 2928.
(14) Kossilick, H.; Lischke, G.; Landmesser, H.; Parlitz, B.; Storek, W.; Fricke, R. *J. Catal.* **1998**, *176*, 102.
(15) Schmidt, R.; Junggreen, H.; Stocker, M. *Chem. Commun.* **1996**, 875.
(16) Romero, A. A.; Alba, M. D.; Klinowski, J. *J. Phys. Chem. B.* **1998**, *102*, 123.
(17) Janicke, M. T.; Landry, C. C.; Christiansen, S. C.; Birtalan, S.; Stucky, G. D.; Chmelka, B. F. *Chem. Mater.* **1999**, *11*, 1342.
(18) Luan, Z.; Hartmann, M.; Zhao, D.; Zhow, W.; Kevan, L. *Chem. Mater.* **1999**, *11*, 1621.
(19) Biz, S.; White, M. G. *J. Phys. Chem. B.* **1999**, *103*, 8432.
(20) Echchahed, B.; Moen, A.; Nicholson, D.; Boneviot, M. *Chem. Mater.* **1997**, *9*, 1716.
(21) Fröba, M.; Köhn, R.; Bouffaud, G. *Chem. Mater.* **1999**, *11*, 2858.
(22) Hartmann, M.; Racouchot, S.; Bischof, C. *Chem. Commun.* **1997**, 2367.
(23) Reller, A.; Ebbinghaus, S.; Köhn, R.; Fröba, M.; Sazama, U.; Fortunato, P. *Mater. Res. Soc. Symp. Proc.* **1999**, *547*, 75.
(24) Morey, M. S.; Stucky, G. D.; Schwarz, S.; Fröba, M. *J. Phys. Chem. B* **1999**, *103*, 2037.
(25) Zhu, Z.; Chang, Z.; Kevan, L. *J. Phys. Chem. B* **1999**, *103*, 2680.
(26) Zhang, Z.; Suo, J.; Zhang, X.; Li, S. *Appl. Catal. A: General 179* **1999**, 11.
(27) (a) Morey, M. S.; Bryan, J. D.; Schwarz, S.; Stucky, G. D. *Chem. Mater.* **2000**, *12*, 3435. (b) Han, Y. J.; Lim, J. M.; Stucky, G. D. *Chem. Mater.* **2000**, *12*, 2068. (c) Morey, M. S.; Davidson, A.; Stucky. G. D. *J. Porous Mater.* **1998**, *5*, 195.
(28) (a) Lin, H. F.; Liu, R. S.; Liew, K. Y.; Johnson, R. E.; Lunsford, J. H. *J. Am. Chem. Soc.* **1984**, *106*, 4117. (b) Mendelovici, L.; Lunsford, J. H. *J. Catal.* **1985**, *94*, 37. (c) Bettahar, M. M.; Costentin, G.; Savary, L.; Lavalley, J. C. *Appl. Catal. A*, **1996**, *145*, 1. (d) Grasselli, R. K. *Catal. Today*, **1999**, *49*, 141.
(29) (a) Tanaka, K.; Takeo, H. Matsumura, C. *J. Am. Chem. Soc.* **1988**, 109, 2422. (b) Kazuta, M.; Tanaka. K. *J. Catal.* **1990**, *123*, 164. (c) Yermakov, Y. I. *Catal. Rev.* **1976**, *14*, 78. (d) Howe, R. F.; Leith, I. R. *J. Chem. Soc., Faraday Trans.1*, **1973**, *69*, 1967.
(30) Muramatsu, A.; Tatsumi, T.; Tominaga, H. *J. Phys. Chem.* **1992**, *96*, 1334.
(31) Sakamoto. Y.; Kaneda. M.; Terasaki. O.; Zhao, D.; Kim. J. M.; Stucky. G.; Shin. H. J.; Ryoo. R. *Nature* **2000**, *408*, 449.
(32) Huo, Q.; Margolese, D. I.; Ciesla. U.; Feng, P.; Gier, T. E.; Sieger, P.; Leon, R.; Petroff, P. M.; Schüth, F.; Stucky, G. D. *Nature* **1994**, *368*, 317.
(33) Huo, Q.; Margolese, D. I.; Ciesla. U.; Demuth, D. G.; Feng, P.; Gier, T. E.; Sieger, P.; Firouzi, A.; Chemelka, B. F.; Schüth, F.; Stucky, G. D. *Chem. Mater.* **1994**, *6*, 1176.
(34) Huo, Q.; Leon, R.; Petroff, P. M.; Stucky, G. D. *Science* **1995**, *268*, 1324.
(35) Huo, Q.; Margolese, D. I.; Stucky, G. D. *Chem. Mater.* **1996**, *8*, 1147.
(36) Stucky, G. D.; Huo, Q.; Firouzi, A.; Chmelka, B. F.; Schacht, S.; Voigt-Martin, I. G.; Schuth, F. *Stud. Surf. Sci. Catal.* **1997**, *105*, 3.
(37) Kim, M. J.; Ryoo, R. *Chem. Mater.* **1999**, *11*, 487.

(38) Kruk, M.; Jaroniec, M.; Ryoo, R.; Kim, J. M. *Chem. Mater*. **1999**, *11*, 2568.
(39) Che, S. A.; Sakamoto, Y.; Terasaki, O.; Tatsumi, T. *Chem. Mater*. **2001**, *13*, 2237.
(40) Kruk. M.; Jaroniec. M.; Sayari. A. *Langnuir* **1997**, *13*, 6267.
(41) Satyari. A.; Liu. P.; Kruk. M.; Jaroniec. M. *Chem. Mater*. **1997**, *9*, 2499.
(42) Jaroniec. M.; Kruk. M.; Sayari. A. *Stud. Surf. Sci. Catal*. **1998**, *117*, 575.
(43) Kruk, M.; Jaroniec, M.; Sakamoto, Y.; Terasaki, O.; Ryoo, R.; Ko, C. H. *J. Phys. Chem. B* **2000**, *104*, 292.
(44) (a) Zhang, W.; Wang, J.; Tanev, P. T.; Pinnavaia, T. J. *Chem. Commun.* **1996,** 979. (b) Tanev, P. T.; Pinnavaia, T. J. *Chem. Mater*. **1996**, *8*, 2068.
(45) Sing, K. S. W.; Everett, D. H.; Haul, R. A. W.; Moscou, L.; Pierotti, R. A.; Rouquérol, J.; Siemieniewska, T. *Pure Appl. Chem.* **1985**, *57*, 603.
(46) V. Luzzati, R. Vargas, P. Mariani, A. Gulik, H. Delacroix, *J. Mol. Biol.* **1993**, *229*, 540.
(47) Weber, R. S. *J. Catal*. **1995**, *151*, 470.
(48) Williams, C. C.; Ekerdt, J. G.; Jehng, J. M.; Hardcastle, F. D.; Turek, A. M.; Wachs, I. E. *J. Phys. Chem.* **1991**, *95*, 8781.
(49) Kumar Rana, R.; Viswanathan, B. *Catal. Lett.* **1998**, *52*, 25.
(50) Jeziorowski, H.; Knöniger, H.; *J. Phys. Chem.* **1979**, *83*, 1166.
(51) Fournier, J.; Louis, C.; Che, M.; Chaquin, P.; Masure, D. *J. Catal*. **1989**, *119*, 400.
(52) Piquemal, J.-Y.; Manoli, J.-M.; Beaunier, P.; Ensuque. A.; Tougne, P.; Legrand, A.-P.; Brégeault, J.-M. *Microporous Mesoporous Mater*. **1999**, *29*, 291.
(53) Clarkson, R. B. *J. Catal.* **1987**, *106*, 505.
(54) Desikan, A. N.; Huang, L.; Oyama, S. T. *J. Phys. Chem.* **1991**, *95*, 10050.
(55) Williams, C. C.; Ekerdt, J. G.; Jeng, J.; Hardzej, F. D.;. Turek, A. M.; Wachs, I. E. *J. Phys. Chem.* **1991**, *95*, 8781.
(56) Hardcastle, F. D.; Wachs, I. E. *J. Raman Spectrosc*. **1990**, *21*, 683.
(57) Collart, O.; Van Der Voort, P.; Vansant, E. F.; Gustin, E.; Bouwen, A.; Schoemaker, D.; Ramachandra Rao, R.; Weckhuysen, B. M.; Schoonheydt, R. A. *Phys. Chem. Chem. Phys*. **1999**, *1*, 4099.
(58) Griffith, W. P.; Lesniak, P. B. *J. Chem. Soc.* A **1969**, 1066.
(59) Aveston, J.; Anacker, E. W.; Johnson, J. S. *Inorg. Chem.* **1969**, *3*, 735.